Int J Fract (2023) 241:171–187
https://doi.org/10.1007/s10704-023-00693-z

RESEARCH

Discrete crack mechanics of disk compression for measurement of low fracture toughness

Mohammad Alabdullah · Andrew Sheng · Nasr Ghoniem

Received: 4 September 2022 / Accepted: 10 February 2023 / Published online: 9 March 2023

Abstract Diametral compression of pre-notched disks is shown to predict the fracture toughness of very brittle materials from the relationship between the crack arrest position and the imposed loading displacement. The discrete crack mechanics method (DCM), which is based on a representation of planar cracks by a discrete set of Volterra dislocations, is used to accurately predict crack growth without re-meshing of the disk geometry as the crack grows. The numerical accuracy of the DCM is demonstrated for 2D and 3D crack geometry. The DCM-predicted crack size when it is arrested is compared to experimental data on alumina (Al_2O_3) and found to be in good agreement. The measured fracture toughness for samples, which contained up to 25% porosity, were found to be 1.99 MPa$\sqrt{\text{m}}$ using a 3D model, and 2.1 MPa$\sqrt{\text{m}}$ from 2D simulations.

M. Alabdullah (✉)
Department of Mechanical Engineering, Kuwait University, Kuwait, Kuwait
e-mail: mohammad.alabdullah@ku.edu.kw

A. Sheng
Xos Trucks, Xos Trucks, Los Angeles, CA, USA
e-mail: asheng89@gmail.com

N. Ghoniem
Department of Mechanical and Aerospace Engineering, University of California Los Angeles, Los Angeles 90095, CA, USA
e-mail: ghoniem@ucla.edu

1 Introduction

Accurate values of the fracture toughness are essential to the prediction of component failure under complex loading and thermal conditions. The need for accuracy is particularly significant when the fracture toughness is low, because measurement errors can result in large uncertainties in determining failure loads. Ceramics and refractory metals are attractive materials for their ability to maintain high strengths during prolonged exposure to elevated temperatures in harsh environments. However, a drawback that is characteristic of ceramics is their tendency to fracture unpredictably. Refractory metals typically have low ductility at low temperatures and tend to be sensitive to impurity content. It is interesting then to realize that materials that are developed for extreme temperatures are typically endowed with low fracture toughness. This aspect poses a challenge when measuring properties, such as tensile and flexural strengths and fracture toughness, through the traditional bending test. Premature fracture failure can occur due to the presence of even very small surface defects, which invalidates the measured strength. Additionally, tensile tests on low fracture toughness materials are not reliable because of the difficulty in preparing specimens and the high chance that they would break in the grips. Specimens must also be perfectly aligned to avoid any bending stresses.

The diametral compression (DC) test has been used as an alternative method for measuring the strength and

toughness of brittle materials or materials that are difficult to adapt to traditional bending tests Sheity et al. (1985), Zaytsev and Panfilov (2014), Es-Saheb et al. (2011), Jonsén et al. (2007), Mazel et al. (2016). Moreover, Elastic properties such as Young's modulus and shear modulus along with Poisson's ratio can also be extracted from DC test especially when combined with digital image correlation (DIC) to achieve more accurate displacement field measurements Liu et al. (2021). The test can also be used to determine the fracture toughness of materials by introducing a small pre-crack prior to loading the specimen Awaji and Sato (1978), Awaji and Sato (1979), Szendi-Horvath (1980), Clobes and Green (2002), Croquelois et al. (2021). More recent work by Newton et al. has shown that the Brazilian nut test can also be used to determine the inter-laminar tensile strength of ceramic matrix composites Newton et al. (2022). The testing procedure involves placing the disk between two platens and applying a compression load in the direction of the diametral axis. This results in a localized region of tensile stress perpendicular to the loading direction at the center of the disk. The applied load is increased until fracture occurs, at which point the strength or toughness of the material can be determined. Clobes and Green showed that the fracture toughness can be estimated from DC tests alone for simple specimen/crack geometries using readily-available analytical solutions for the disk stress and stress intensity factor Clobes and Green (2002).Sabri has also shown that mode I and mode II fracture toughness can be determined through DC test with a simple geometry crack induced to the specimen disk Sabri et al. (2016). However, in cases in which analytical stress intensity factor solutions are not available for the crack shape (especially for 3D crack geometries), estimating the fracture toughness becomes more difficult, requiring accurate numerical solutionsZakavi et al. (2022). In general, analytical solutions for the elastic field of a crack are only available for problems involving simple geometry and loading conditions. However, it is necessary to use a computational method if the geometry or the crack shape are not simple, or when an analytical solution is not available. For example both the finite element method (FEM) Shin and Cai (2004) and the boundary element method (BEM) Yan (2006) were used widely to estimate stress intensity factors for complex crack/specimen geometry. One concern in existing computational approaches, based on the FEM, is the need to employ a very fine mesh around the crack tip, and then re-mesh the whole body as the crack propagates. Another approach in fracture mechanics is the concept of dislocation-based representation of cracks, which can be traced back to Eshelby Eshelby (1982). Here, a crack may be described as a displacement jump smoothly distributed along the crack plane. In other words, a crack may be considered a type of Somigliana dislocation Eshelby (1982). Eshelby, Frank, and Nabarro then showed that a pileup of discrete Volterra-type dislocations with a fixed Burgers vector could be used to create a stepped approximation of a crack Eshelby et al. (1951).

We develop here a procedure to simulate crack propagation during the DC test using the Discrete Crack Mechanics (DCM) method, in which cracks are modeled with discrete Volterra dislocation arrays. The method is based on the work of Ghoniem and coworkers, who adapted the Parametric Dislocation Dynamics (PDD) method to calculate the elastic field of complex 3D cracks Ghoniem et al. (2000), Ghoniem and Huang (2006). This work was further extended to simulate fatigue fracture in finite geometry by Takahashi and Ghoniem, who also showed that the method can be used to calculate the stress intensity factor for a crack Takahashi and Ghoniem (2013). Recently, an equation of motion governing crack dislocations during critical crack growth has been developed and implemented within the DCM framework to model critical crack growth Sheng et al. (2018). It will be shown that by reproducing the DC test conditions in a DCM simulation, the fracture toughness of a material can be accurately determined.

When a load is applied to compress the disk that contains a single dominant crack, it initially acts as a spring that stores elastic energy. Once the disk fractures in a controlled manner, part of this stored energy is consumed in opening up the crack faces, while the remainder is stored elastically in the surrounding material. For a given fracture toughness, partitioning of these two types of energy (elastically stored and crack opening energy) is determined by one single parameter, and that is the final arrested crack size. We propose here that measurement of the arrested crack size for a specific applied displacement will uniquely determine the fracture toughness. Hence, with a quick optical observation, one can accurately and precisely determine the fracture toughness.

The objective of the present work is to utilize the accuracy of the discrete fracture mechanics (DFM) in

calculations of the Stress Intensity Factor (SIF) for a growing crack in the DC test as a means to determine the fracture toughness when the crack stops. At this point, the SIF is the numerical value of the fracture toughness. To achieve this goal, we first describe the DC test procedure in Sect. 2.1. We then discuss the results of a DC test on an Alumina disk in Sect. 2.2. A 3-D crack model is presented in Sect. 3.1, where a small surface crack grows under the application of an external compression load. The model shows details of its propagation, first through the sample from surface to the opposite surface, and then its expansion along the compressed diameter. Following these observations, we present a simpler 2-D DFM model of the crack in Sect. 3.2. The 2-D model is shown to give similarly accurate values of the fracture toughness at a reduced cost of computations. In Sect. 4, results for fracture toughness measurements are shown. Here, the computational information on crack length is compared to its measured size to determine the fracture toughness. Finally, conclusions are given in Sect. 5.

2 Experiments

2.1 Testing procedure

A 25.4 mm diameter bisque-fired 96% alumina rod (502–1400-BF, Aremco, Valley Cottage, NY) was cut into 6.35 mm thick disks to be used for the diametral compression tests. According to the manufacturer, the density of the specimen material is 3.0 g/cm^3 giving a porosity of 25%.Unlike fully-dense alumina, the porosity in our samples is considerably higher. In fact, to qualify for structural engineering applications, alumina must be at least has 80% Al_2O_3, with no open porosity. At room temperature the porosity cannot exceed 6% for structural applications. Alumina is categorized into 9 grades (A1-A9), with A1 has the least porosity and higher percentage of Al_2O_3Auerkari (1996). The alumina rods used in this work were bisque fired at 2475 F and according to the manufacturer, additional strength and higher density can be achieved when bisque fired at 3000–3125 F. The elastic modulus, Poisson's ratio, and fracture toughness were not available from the manufacturer. The disk faces were finished by a rough grinding procedure using 100 and 240-grit SiC sandpaper, followed by fine polishing with 600-grit sandpaper to minimize extraneous surface defects that could serve as crack initiation sites. A set of inconel platens were used to compress the disks, with each platen having a radius of 15.875 mm and a 73.74° arc as shown in Fig. 1a.

To avoid the initiation of secondary cracks often observed in diametral compression tests Swab et al. (2011) and to encourage the growth of a single central crack, semi-elliptical surface notches $2c = 8$ mm in length and approximately $a = 1.5$ mm in depth were introduced using a razor blade (0.4 mm thickness) with a V-shaped edge on a single face of each sample, as shown in Fig. 1b. The notches serve as stress-concentration sites to encourage crack growth along a specific plane and are often used in diametral compression tests to measure fracture toughness Szendi-Horvath (1980), Clobes and Green (2002), Gopalakrishnan and Mecholsky (2012).

An Instron Series 5880 universal testing machine was used to apply compressive loads on the platen/disk assemblies. Bluehill 2 software was used to apply a compressive displacement to the specimens at a rate of 0.005 mm/s. The criterion used to signal the end-of-test was when the load fell below 20% of the maximum compressive load measured in the final 100 ms of the test. The software also used to record the real time load–displacement curve during each test. The elastic modulus and Poisson's ratio were calculated according to the compressive loads and displacements measured during the tests. The loads were obtained using an Instron 2525-801 load cell and the displacement and strain fields were obtained using digital image correlation (DIC) performed using open-source Matlab-based DIC software (Ncorr Blaber et al. (2015)).It is worth mentioning that the speckle pattern was generated using a speckle generator - correlated solution software, where a pattern can be generated based on input related to density, size and randomness Solutions (Solutions), Blaber et al. (2015). The optimum speckle parameters (speckle diameter = 0.063 mm, speckle density = 55% and variation = 70%) were used after running a sensitivity analysis, where the alumina elastic modulus measurements was considered as reference and compared with values reported in the literature Auerkari (1996).

2.2 Diametral compression test results

Six tests were carried out using six alumina disks cut from the same rod obtained from the manufacturer (Aremco). The disks had the same density, porosity and

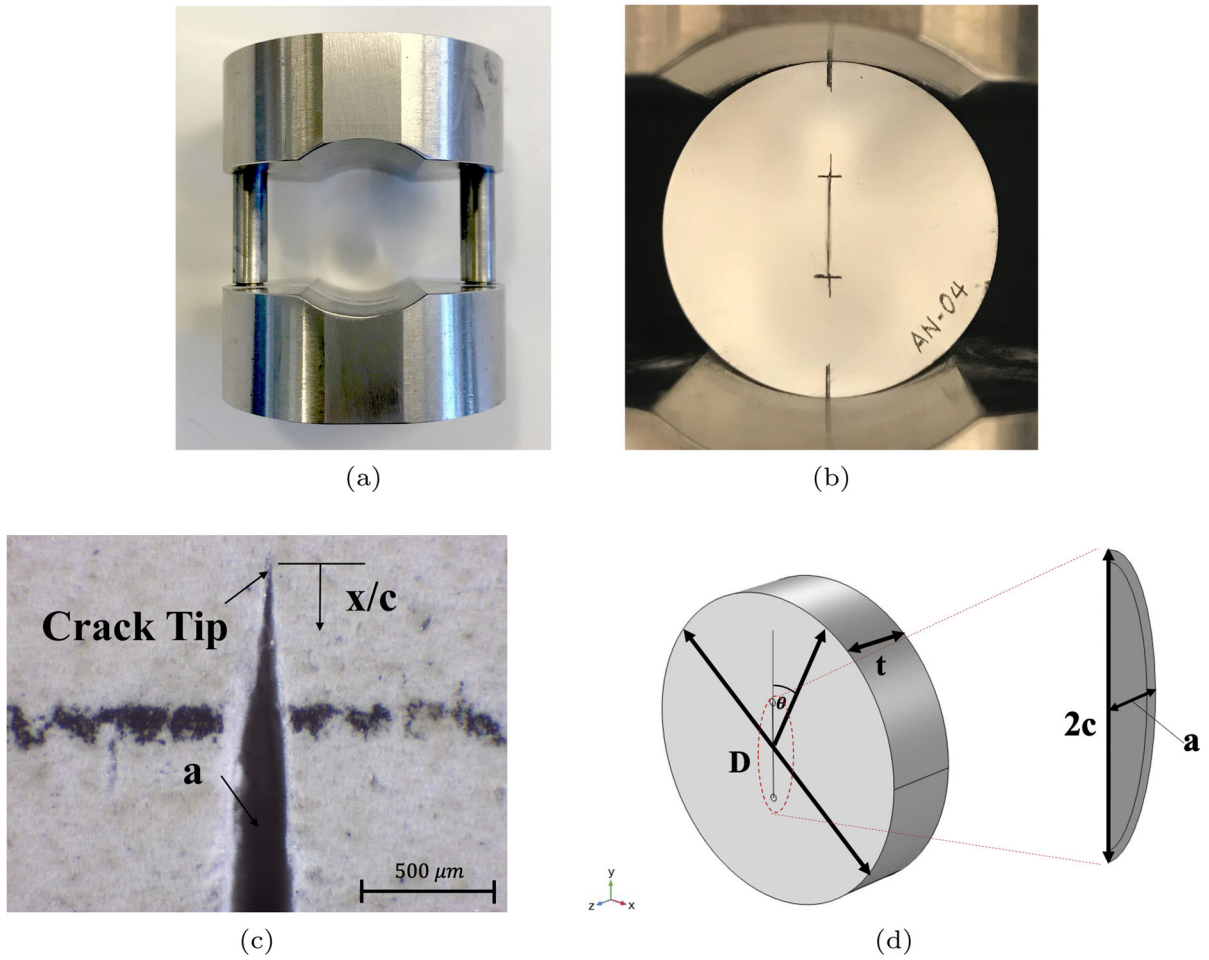

Fig. 1 **a** Circular Inconel platens used to compress sample disks. **b** Pre-notched Al_2O_3 sample disk mounted between the circular platens. The vertical and horizontal markers are for alignment purposes. **c** Microscopic picture of the Induced crack tip. **d** Specimen and crack geometry illusteration

elastic properties. For each test, the stress at the center of a diametrically-compressed disk was estimated using the instantaneous load measured by the load cell with the equation Fahad (1996):

$$\sigma_f = \frac{2P}{\pi Dt}\frac{(\sin 2\theta - \theta)}{\theta} \tag{1}$$

where D is the disk diameter, t its thickness, and 2θ is the angle subtended by the contact patch. Due to the compliance of the testing frame and platens themselves, only loads used in the linear region of the load–displacement curve were used in the elastic modulus calculations. A typical load–displacement curve for the tests performed with unnotched specimens is shown in Fig. 2.

DIC images were automatically taken every 3 s during the test and the corresponding load recorded. Typical strain fields obtained from the DIC software are shown in Fig. 3. The elastic modulus of the tested alumina was determined to be $E \approx 231.52$ GPa, based on the diametral tensile stress σ_{xx} calculated using equation 1 and the corresponding strain component ε_{xx} from the DIC analysis. The measured value of E is in the range reported for alumina, grade A9 Auerkari (1996).

The average cross-head displacement at failure was 0.285 mm, corresponding to an average fracture load of 3.8 kN. A main central crack was observed in all specimens to have propagated through the specimen thickness, with the crack growing symmetrically across the

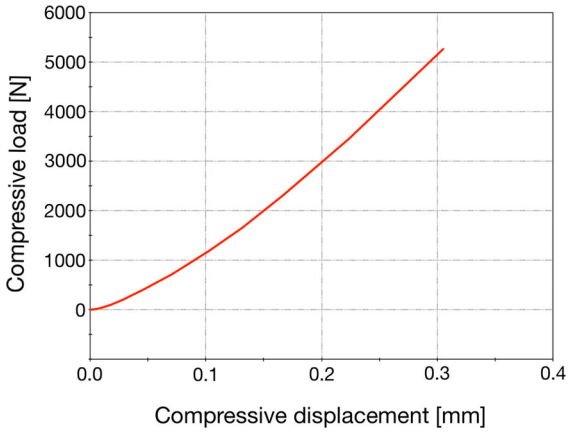

Fig. 2 Load–displacement curve for an un-notched specimen before failure (fails at 5.3 kN)

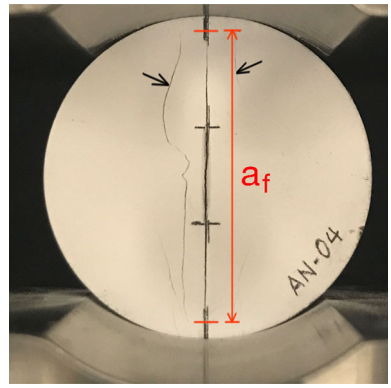

Fig. 4 Specimen at the end of the DC test, where the final crack size is marked. Note the presence of secondary cracks, which were initiated after the central crack reached its final length

mid-plane to an average length of $2c_f = 22.86$ mm. It was expected that the main crack stops near the disk poles due to the nature of the stress field distribution in the disk compression test. The imposed contact boundary conditions create highly compressive stress regions near the poles, which will eventually stop the crack originating from the imposed notch. In fact, the diametral compression test was intentionally selected for the purpose of measuring the fracture toughness of alumina, since our measurement depends on the fact that the imposed crack propagate in a controllable manner and stops when equilibrium between the driving Peach-Koehler force and the matrix fracture toughness is achieved. In some specimens, secondary cracks were formed on either side of the main central crack, as indicated by the black arrows in Fig. 4. Comparisons between the test results and the model predictions suggest that the secondary cracks are formed after the central crack reached its final length. This conclusion is discussed in further details in Sect. 4.

Carpinteri et al. Carpinteri (1991) developed the following expression for the stress intensity factor of a semi elliptical crack (depth a and width 2c) under tension in a beam (height 2 h) with a rectangular cross-section (width w and depth b).

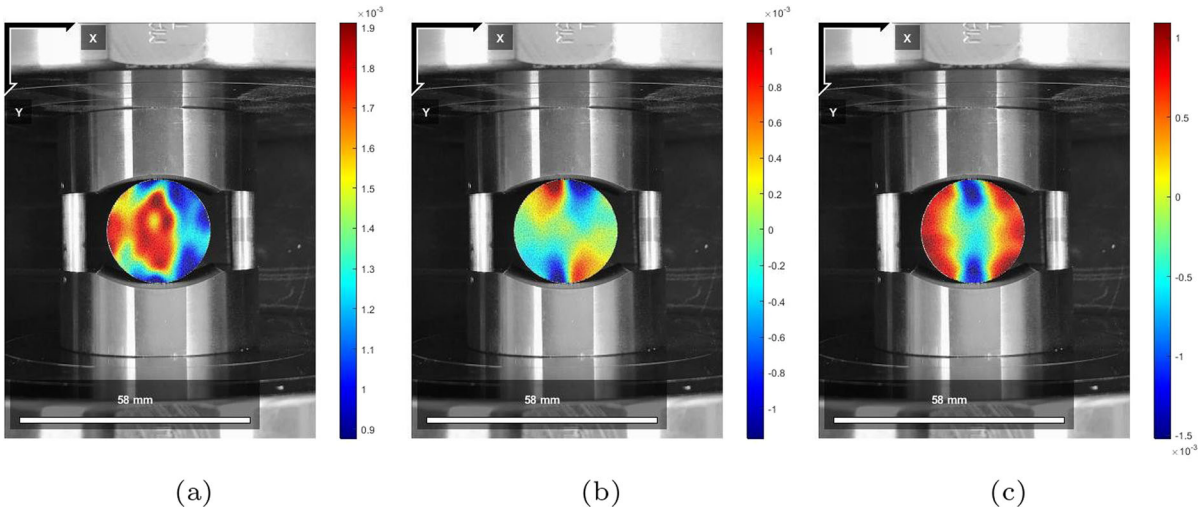

Fig. 3 Strain components (**a**) ε_{xx}, **b** ε_{xy}, and **c** ε_{yy} before fracture at approximately 5.3 kN in an un-notched specimen obtained using DIC

$$\frac{K_{I,i}}{\sigma_F\sqrt{\pi a}} = \frac{Y_F(\zeta_i)}{1 + 2p(\zeta_i)\frac{b}{h}(\frac{1}{2} - \frac{c}{w}) - 2\frac{c}{w} + \frac{\Delta c}{w}(h + bp(\zeta_i))\sum_{j=1}^{n}\frac{1}{h+bp(\zeta_i)}} \tag{2}$$

where σ_f, ζ_i, Δc, $p(\zeta_i)$ and $Y(\zeta_i)$ are the applied uniaxial stress, a_i/b relative crack depth of the ith element, crack width segment increment, dimensionless local axial compliance and polynomial function of the relative crack depth, respectively. The developed expression approximates the stress intensity factor by dividing the semi elliptical crack into discrete strips arranged in series and parallel of through-thickness edge cracks as shown in Fig. 5a Carpinteri (1991). Moreover, the expression deals with semi elliptical cracks with aspect ratios (a/c) that vary from 0.2 to 1.0 while the relative depth ($\zeta = a/b$) of the crack deepest point is assumed to be lower than or equal to 0.6. Based on this analysis, the largest stress intensity factor occurs at the deepest part of the semi-elliptical crack. Assuming that crack growth initiates here, the fracture toughness of the alumina disks is found to be approximately 1.99 MPa$\sqrt{\text{m}}$. The estimated stress intensity factor distribution along the crack tip is shown in Fig. 5b.

From this estimation of the stress intensity factor along the crack tip, it can be hypothesized that the crack initially grows quickly towards the back surface before spreading along the faces of the disk.

3 Discrete crack mechanics (DCM) models

In the discrete crack mechanics (DCM) method, cracks are constructed using Volterra dislocation loops. The method allows for the natural introduction of displacement discontinuities, thus eliminating mesh dependence in modeling crack growth. The elastic field of cracks in finite bodies is separated into two parts: the infinite-medium solution of discrete dislocations and a finite element method solution of a correction problem that satisfies external boundary conditions. In the DCM, a crack is represented by a dislocation array with a fixed outer loop determining the crack tip position encompassing additional concentric loops free to expand or contract. Solving for the equilibrium positions of the inner loops gives the crack shape and stress field. Details of the method can be found in our earlier publications Takahashi and Ghoniem (2013); Sheng et al. (2018).

3.1 DCM-3D model

The disk compression test model consists of a mesh representative of the alumina disk specimens in contact with two perfectly rigid circular platen surfaces at the top and bottom surfaces of the mesh. The disk has a diameter of 25.4 mm and a thickness of 6.35 mm while the circular platens have radii of 15.875 mm and 73.74° arcs to match the experimental conditions. A semi-elliptical surface crack with a semi-major axis of 8 mm and a semi-minor axis of 1.65 mm was inserted parallel to the loading direction as shown in Fig. 6. A downward displacement of 0.034 mm is prescribed for the upper platen while the same displacement is applied in the upward direction for the lower platen. Note that there is no mesh refinement in the region surrounding the crack, as the superposition method eliminates the need for any special meshing schemes.

To ensure that the disk is not over-constrained, a contact problem based on the penalty method was set up for the DCM simulation of a diametral compression test. The upper and lower boundaries are defined to represent the displaced platen surfaces, and surface mesh nodes for which interpenetration is detected are identified. A repulsive force proportional to the amount of interpenetration is applied to these nodes in order to enforce proper contact conditions. Since the contact boundary and forces are unknown, the solution must be evaluated iteratively. It is assumed that no relative motion occurs between the disk and platen surfaces.

3.2 DCM-2D model

As an alternative approximation to 3D Volterra dislocation loops representing the crack, we also developed a 2D version of the DCM method that is less computationally demanding, yet gives good approximations in cases where the crack shape is more elongated along one direction. We note from the 3D results that as soon as the surface crack penetrates the specimen, it elongates considerably along the loading axes. It is therefore instructive to investigate the accuracy of the results

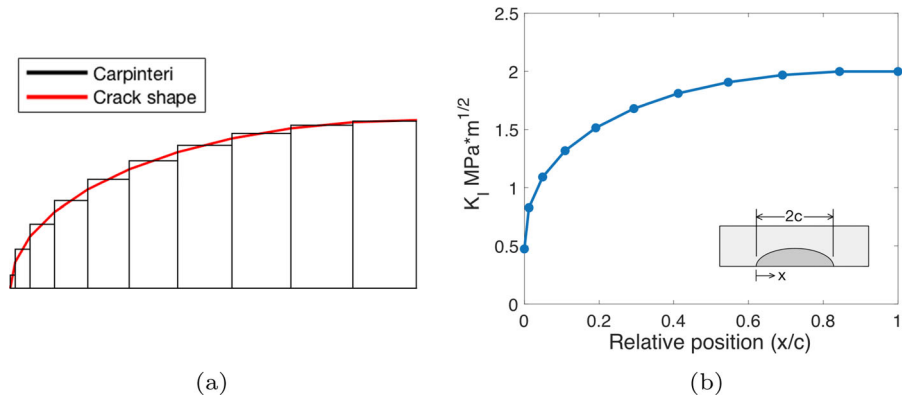

Fig. 5 **a** Carpinteri's approximation method for an elliptical crack. **b** Predicted stress intensity factor along the crack tip

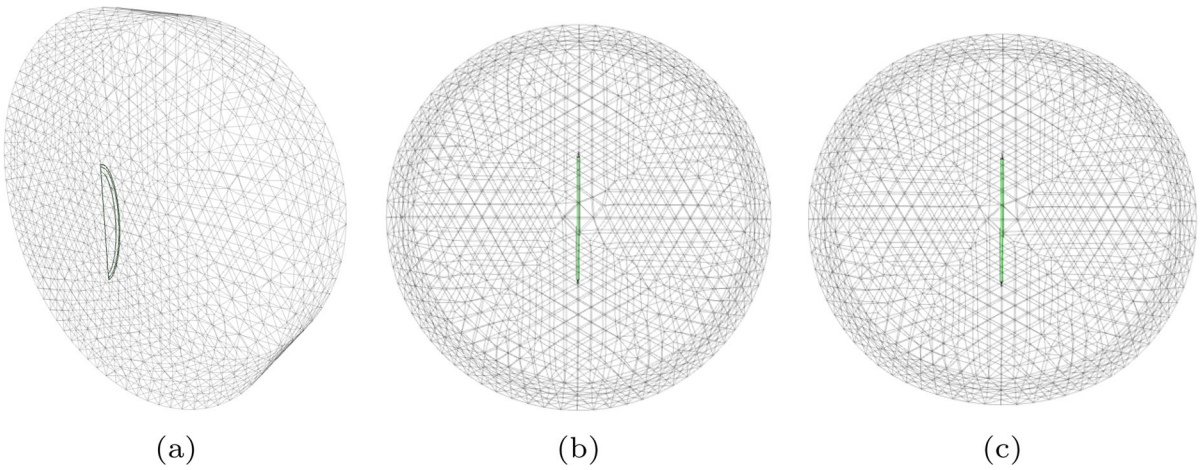

Fig. 6 **a** Crack dislocation loops in an elliptical surface crack configuration. Meshes show (**b**) undeformed and **c** deformed disk geometry

when we compare the 3D solution to that of a 2D propagating crack.

2D analysis of the DC test was carried out utilizing the FEM commercial software COMSOL in conjunction with a Matlab code that calculates the stress field of dislocations in 2D. In this analysis, we considered infinitely long Volterra dislocation loops represented as dislocation dipoles. Edge dislocations represent mode-I crack, with their Burgers vector oriented perpendicular to the crack surface, as shown in Fig. 8a. The infinite medium solution of discrete dislocations was provided by the developed 2D DCM Matlab code, while the FEM solution of the correction problem was obtained from COMSOL Multiphysics. Using the superposition technique Sheng et al. (2018), we readily obtain the elastic field of the crack in the finite domain of the alumina disk.

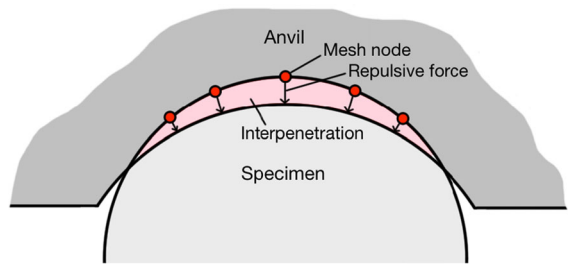

Fig. 7 Contact model for enforcing platen-specimen contact conditions. The repulsive force is proportional to the distance between Anvil and specimen nodes

The 2D FEM simulation was set up as a plane stress problem, along with contact forces at the common interface between the disk and platens. The contact conditions used for the 2D COMSOL model were set to the penalty method. Appropriate values for the penalty fac-

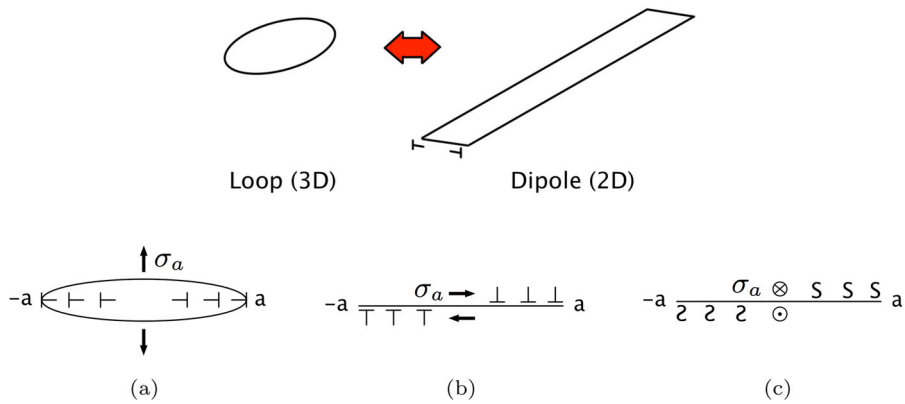

Fig. 8 (Top figure): Equivalence between 3D dislocation loops and 2D dislocation dipoles. Dipole representation of (a) Mode-I crack (climb edge) (b) Mode-II crack (glide edge) (c) Mode-III crack (screw)

tors were determined through validation of the stress field given by equation 1. Both the alumina disk and the platens were modeled in 2D, where a prescribed displacement boundary condition of a magnitude of 0.0575 mm was applied to the top and bottom platens, as shown in Fig. 9. Similar to the 3D model, a contact problem based on the penalty method was utilized. Moreover, and to ensure traction free surfaces, distributed tractions $-\boldsymbol{t}^{\boldsymbol{d}}$ and displacements $-\boldsymbol{u}^{\boldsymbol{d}}$ were applied at the disk boundary and platens contact surfaces, respectively, as shown in Fig. 9. These tractions and displacements were computed from the stress and displacement fields of all dislocation dipoles within the crack, $\boldsymbol{t}^{\boldsymbol{d}} = \boldsymbol{\sigma}^{\boldsymbol{d}}.\boldsymbol{n}$, where $\boldsymbol{t}^{\boldsymbol{d}}$ and $\boldsymbol{\sigma}^{\boldsymbol{d}}$ are the traction and the corresponding stress resulting from dislocation dipoles. Superposition of the dislocation field solution and the FEM solutions satisfies all boundary conditions corresponding to the experiment.

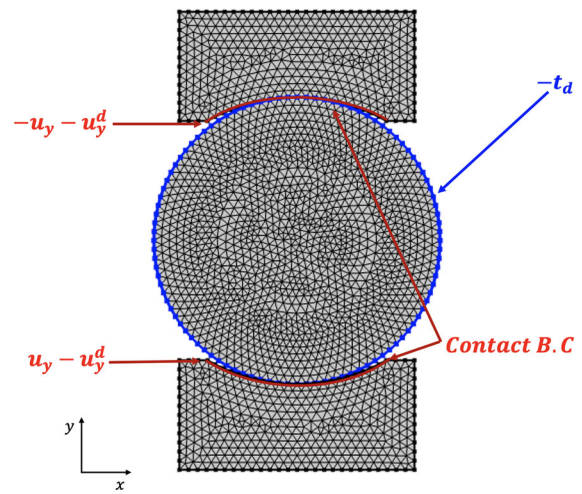

Fig. 9 2D FE model boundary conditions

4 Fracture toughness determination

The fracture toughness of the tested disk will now be determined by computer simulations, where we use the accurate 3D crack representation first and then compare the results to 2D DCM and to full FEM numerical solutions. The simulation procedure proceeds as follows.

4.1 Numerical procedure

First, a dislocation loop (3D) or a pair of leading (fixed) dislocations (2D), separated by a distance equal to the initial crack length, are introduced. This can be considered as a rough approximation of the initial crack shape. To improve accuracy, another dislocation loop (3D) or a dipole (2D) that is free to expand or contract along the crack plane is then placed inside the fixed dislocation loop (3D) or dipole (2D). Subsequently, the entire system of dislocation loops (3D) dipoles (2D) is allowed to come to force equilibrium. This is achieved by incrementing the position of a dislocation node (or dipole), based on a specified maximum displacement dx_{max} per crack growth step. The Peach-Koehler (PK) force on a dislocation node is then calculated and its velocity is obtained. A maximum simulation time step dt_{max} is next calculated based on the specified dx_{max} and the maximum dislocation node velocity. Note that these simulations are carried out for a quasi-static propagating crack, and hence the time variable is in reality an iteration index for the crack to achieve successive quasi-equilibrium shapes. All trailing dislocation particles (nodes) are then moved by a distance given by

the product of dx_{max} and the velocity calculated again for each node. Once the free dislocations have reached their equilibrium positions, a new dipole or dislocation loop is seeded inside the previous one, and the system is again allowed to come to equilibrium. The process is repeated until the applied load is no longer sufficient to support any additional dislocations that can be inserted inside the crack.

Once the final crack shape is found, the stress intensity factor (SIF) along the fixed dislocation is calculated. If it exceeds the fracture toughness, the crack tip dislocation is advanced. Figure 17 illustrates crack growth as described here, under a 0.0575 mm prescribed displacement to the platens. The corresponding computed stress intensity factor at the crack tip is also shown. The figure shows that there is a sharp increase in the computed SIF as the crack progress. However, the rate of crack growth decreases as the crack length gets closer to its final shape. Finally the SIF decreases sharply, reaching a value below the material's fracture toughness. The crack eventually stops growing, and the final crack length is obtained. The main point here is that the equilibrium crack length is obtained, where all PK forces are nearly zero, and the net force on the leading dislocation is also nearly zero (the difference between its PK force and the fracture toughness). Comparing this value of the crack length to its experimental value (22.86 mm), one can readily determine the fracture toughness as 1.99 MPa$\sqrt{m}$ from the 3D calculations. The results of 2D calculations give a value of the fracture toughness of 2.1 MPa$\sqrt{\text{m}}$. The error in obtaining the fracture toughness from 2D calculations is only around 5%. Such error is quite acceptable, given the fact that 2D calculations are much simpler than 3D DFM simulations.

For growing cracks, dx_{max} must be updated at each crack growth step to ensure that a solution can be found. The amount by which dx_{max} is changed is dependent on the crack size - as the crack grows larger, dx_{max} must be increased proportionally. Hence dx_{max} is a function of the crack length. The fracture toughness obtained for the alumina disk using the 2D DCM model was found to be within 5%. The results provided by the simple 2D DCM model can thus be used for quick determination of the fracture toughness without the computational burden of 3D simulations Sheng et al. (2018). The simulated crack shape at four loading intervals during the simulation is shown in Figs. 10 and 11. The initial crack shape, two intermediate shapes, and the final crack shape are shown in the figure. Note that the COD increases as more dislocation loops are inserted. Initially, the crack is semi-elliptical, but becomes more semi-circular as the crack front grows quickly towards the back surface of the disk. Once the crack breaks through the back surface of the disk, it grows along the surface rapidly. As the strain energy in the disk decreases, the crack growth rate near and along the front face decrease accordingly. Eventually the crack takes on a symmetric rectangular shape as the crack dislocations organize into their final equilibrium configuration. As can be seen, during the latter stages of crack growth, dislocation loops look more like elongated dipolar loops that can be modeled in 2D as discussed earlier. The final crack length (taken to be the average distance between the upper and lower crack tips) predicted by the 3D DCM model was 22.84 mm, which is in excellent agreement with the final crack length measured in DC tests.

The stress component (σ_{22}) on the front face of the disk and the mid plane are shown for three simulation steps in Figs. 12 and 13. The figures compare the stress field on the midplane in the initial configuration to the field along the front face. Initially, the crack does not intersect the midplane of the disk so the tensile stress region in the center of the disk is uninterrupted. On the front face, there is no stress in the region corresponding to the notch. At 12,500 steps, the crack has propagated through the midplane, relieving some of the tensile stress. Note the similarities between the stress field on the midplane and front face at the intermediate and final simulation steps.

4.2 Comparison between DFM and FEM

The stress intensity factor calculated along the fixed crack tip dislocation is compared to Carpinteri's analytical approximation in Fig. 14a. The large relative error of 242% at the crack end $x/c = 0$ is possibly due to Carpinteri's approximate edge-crack representation of the 3D elliptical crack. At the end where the relative error is high, the strip approximation is less representative of the true crack shape, as shown in Fig. 5a. The relative error decreases to about 5% at the middle of the crack $x/c = 1$, where the crack tip is more closely approximated by edge crack strips.

We then performed 2D simulations for exactly the same 3D model in order to determine how close the

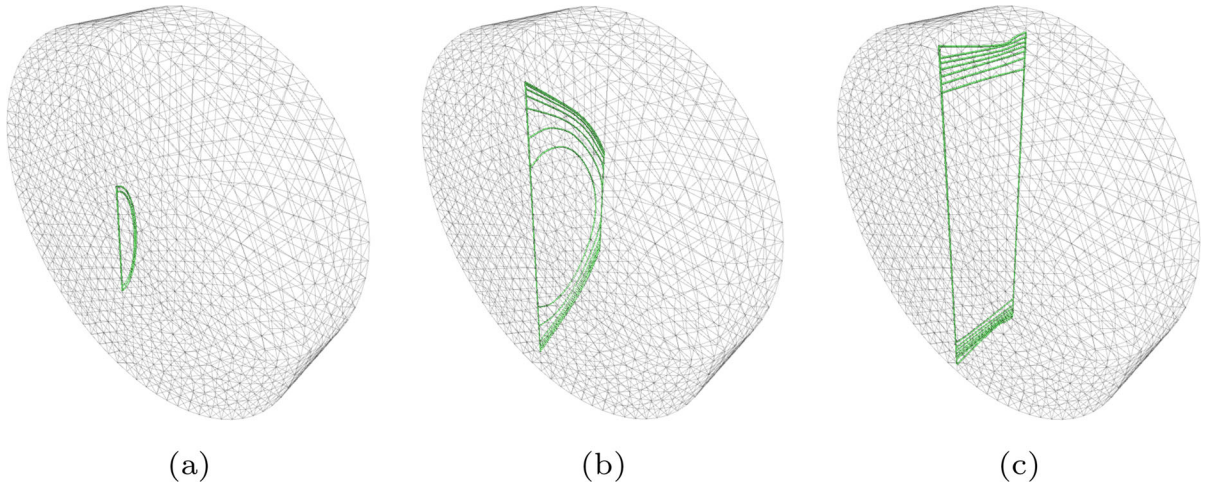

Fig. 10 Configuration of Volterra dislocation loops representing the 3D crack after **a** 100 simulation (loading) steps (initial crack shape), **b** 12,500 steps, and **c** 36,000 steps (final crack shape)

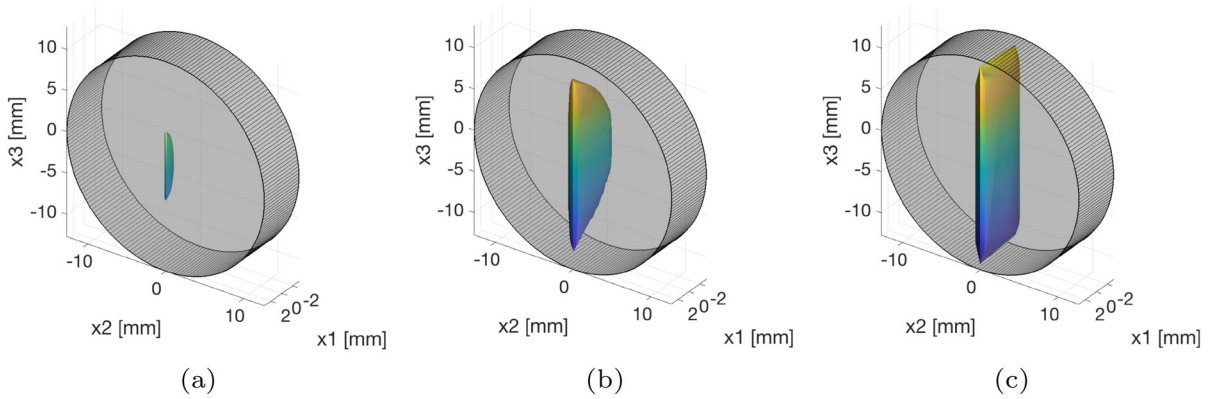

Fig. 11 Predicted crack shape at **a** 100 simulation steps (initial crack shape), **b** 12,500 steps, and **c** 36,000 steps (final crack shape)

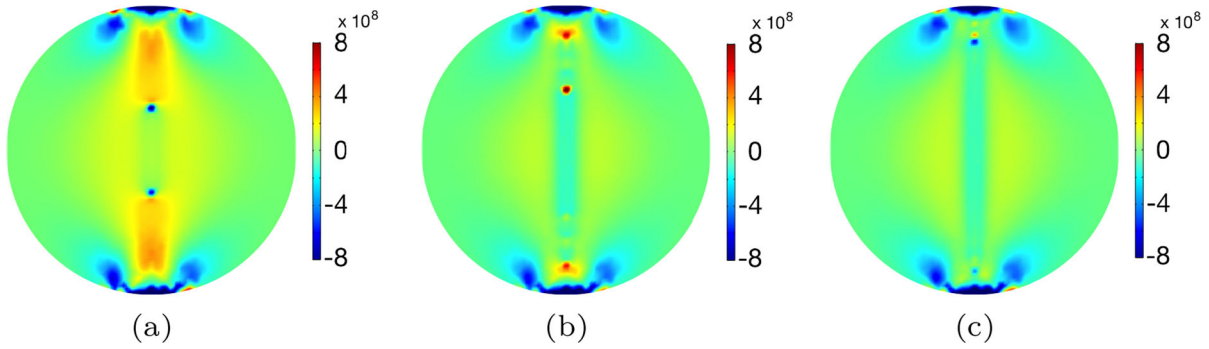

Fig. 12 Crack opening stress component (σ_{22}) on front disk face at **a** 100 simulation steps (initial crack shape), **b** 12,500 steps, and **c** 36,000 steps (final crack shape)

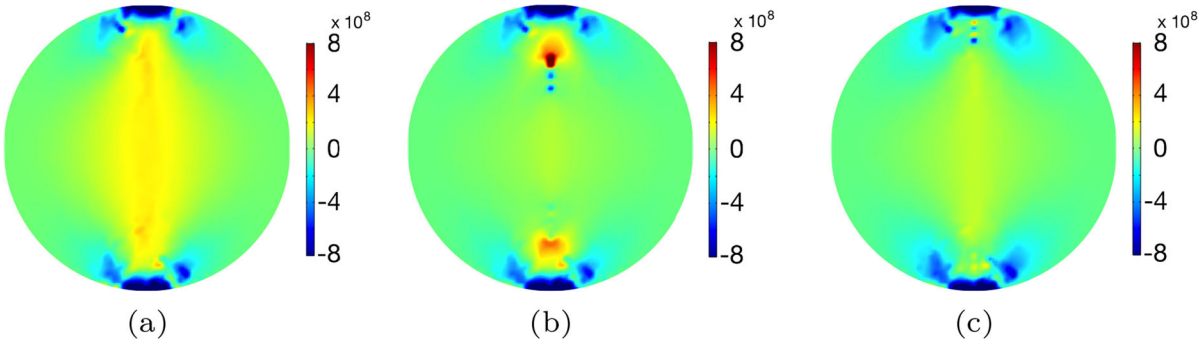

Fig. 13 Crack opening stress component (σ_{22}) on the mid-plane at **a** 100 simulation steps (initial crack shape), **b** 12500 steps, and **c** 36000 steps (final crack shape)

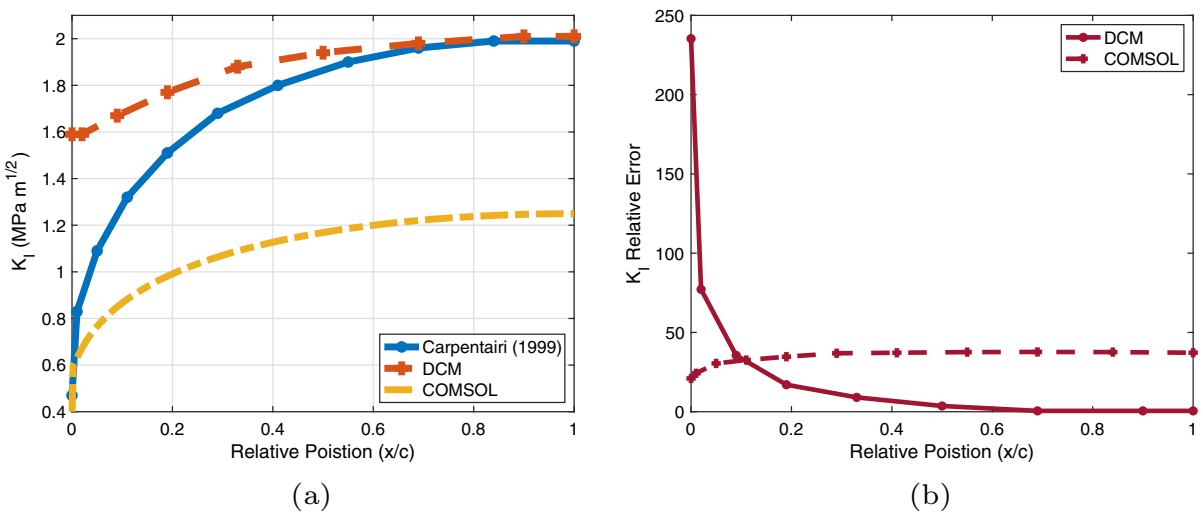

Fig. 14 **a** Stress intensity factor along the crack tip calculated using 2D DCM compared to Carpinteri's analytical approximation and COMSOL numerical solution. **b** Relative K_I error

Fig. 15 Predicted crack shape obtained from 2D DCM model at **a** the initial simulation step (initial crack shape), **b** intermediate simulation step, and **c** final simulation step (final crack shape)

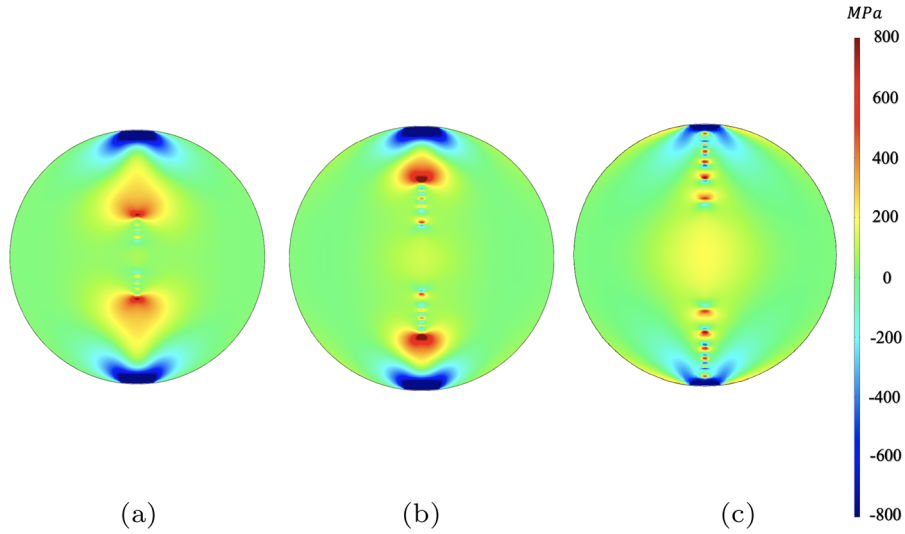

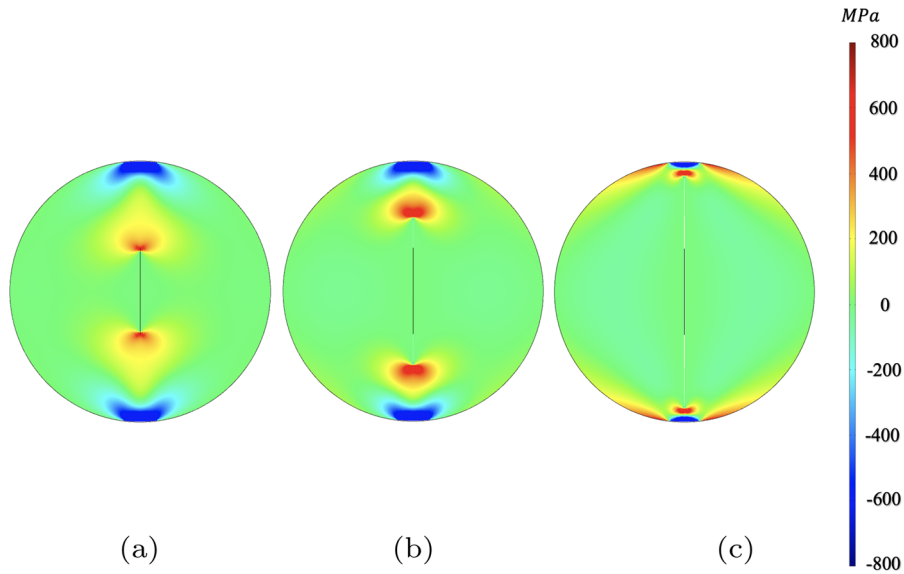

Fig. 16 Predicted crack shape obtained from COMSOL at **a** the initial simulation step (initial crack shape), **b** intermediate simulation step, and **c** final simulation step (final crack shape)

results may be with a simpler computational tool. The final crack length obtained from simulations with the 2D model was 23.4 mm, which is very close to the value obtained from the 3D model (within 2%), and in good agreement with the the experiment. Figure 15 displays the stress evolution in the disk (σ_{22}), as the crack position adjusts to the imposed loading. The crack is represented by only eight pairs of dislocation dipoles.

To ascertain the quality of the results produced by DCM simulations, we compare to calculations obtained from off-the-shelf commercial FEM codes. We will use the COMSOL Multiphysics computer program in order to further verify the model and shed light on its advantages. Recent versions of COMSOL Multiphysics includes different tools that deal with discrete crack propagation and estimation of stress intensity factors. In this section, 2D DCM results of the diametral compression problem will be compared to those obtained purely via COMSOL Multiphysics through the newly introduced discrete crack feature.

A 2D plane stress contact problem based on the penalty method was utilized where a slit was introduced to the disk's front surface representing a 8 mm crack. A crack feature was added to the solid mechanics physics with the crack edge selected and a J-integral sub-node was added in order to compute the J-integral, which is path-independent, around the crack tip. It is worth mentioning that the J-integral contour size variation does not have a significant effect on the J-integral calculation, except when the crack approaches the disk boundaries. In this case, one must be careful so that the contour remains with the disk boundaries. For a crack extending along the positive x-axis, the J-integral is defined as

$$J = \int_{\Gamma} W d_y - T_i \frac{\partial u_i}{\partial x} ds \tag{3}$$

where W is the strain energy density and T is the traction vector. One can relate Mode I stress intensity factor in the case of linear elastic material that satisfies plane stress conditions to the J integral through the following relation: $J = \frac{K_I^2}{E}$, where E is Young's modulus. A parametric sweep was then preformed on the crack length through a series of stationary studies.

Figure 16 shows the stress component σ_{xx} obtained through COMSOL simulation using its crack modeling feature. The results shows good agreement with those obtained in our 2D DCM (Fig. 15). However, as the crack develops closer to the desk's boundaries, a discrepancy in the stress distribution can be noticed, especially at the top and lower bottoms of the boundaries. In order to thoroughly compare the two solutions, stress intensity factors and energy release associated with the crack extension were also compared.

Figure 17a shows a comparison between the stress intensity factor K_I evolution as the crack extends obtained from the 2D DCM method, and from 2D COMSOL numerical solutions. K_I factors show good agreement at the early stages of crack development.

However, the two factors diverge rapidly as the crack extends beyond a total length of 14 mm. One can understand the poor accuracy of the COMSOL crack model when one realizes that the stress singularity around the crack tip is better captured by our DCM method, as shown in Fig. 18. This is a consequence of the fact that in the DCM method, the crack is represented by a discrete set of dislocations dipoles, which already have singular elastic fields. The 2D DCM method also captures the decrease in the SIF as it approaches the disk boundary to a point where the SIF value becomes lower than the material's fracture toughness. At this point, equilibrium is achieved and the resulting half crack length 11.7 mm (2a = 23.4 mm) is in good agreement with the experimental results. On the other hand, The SIF obtained from COMSOL through numerical calculations of the J-Integral shows a decrease as it approaches the boundary. However, the results obtained from COMSOL contradict with experimental observations, since the SIF does not decrease to a level that allows crack arrest. Moreover, The results obtained from COMSOL agrees with the published results from COMSOL example of a central crack in a finite plate under tension Solutions (2020). The example indicated that COMSOL numerical solution over estimated the mode I SIF by 20% when compared with the available analytical solution $K_I = \sigma\sqrt{\pi a}$. On the other hand DCM showed high accuracy levels when compared to these analytical solutions as indicated in reference Sheng et al. (2018).

The energy release rate associated with the crack development has been numerically calculated and compared in both methods as shown in Fig. 17b. For a linear elastic material, $G = J$ where G is the energy release rate. it is possible to compute the value of the J-integral without using the path integrals since

$$G = -\frac{1}{t}\frac{\Delta U}{\Delta(2a)} \tag{4}$$

where U is the potential energy, a is the half crack length, and t is the thickness. Through computing the potential energy for two slightly different crack lengths the energy release rate can be estimated, hence the J integral. Here, the potential energy can be computed from the following relation

$$U = \frac{1}{2}\int_{\Omega} \boldsymbol{\sigma} : \boldsymbol{\epsilon}\, dV - \int_{\partial\Omega} \boldsymbol{T}\cdot\boldsymbol{u}\, dS \tag{5}$$

where the first term on the right represents the elastic energy stored in the volume and the second term represents the potential energy of the prescribed tractions on the boundary.

Thus, The change in potential energy can be calculated, hence the energy release rate (equation 4), at different crack lengths using either the strain energy or the potential energy due to prescribed tractions independently. The energy release in the 2D COMSOL was calculated using the method above and the result was in good agreement with the numerically calculated J-integral through integral paths in COMSOL. On the other hand, the strain energy in the energy release rate in 2D DCM was calculated from the elastic energy of the dislocation dipoles, as:

$$U = -\frac{1}{2}\left(\int_{\Omega} \boldsymbol{\sigma} : \boldsymbol{\epsilon}\, dV + \frac{\mu b^2}{2\pi(1-\nu)} ln(\frac{x_0}{r_0})\, L\right) \tag{6}$$

where μ, b, x_0, N, L and r_0 are the shear modulus, burgers vector, distance between the opposite dislocations, number of dislocation dipoles, dislocation line length and the dislocation core radius ($r_0 = b$), respectively. The first and second terms on the right represent the strain energy obtained from the FEM solution (COMSOL) and the strain energy approximation of edge dislocation dipoles for plane stress. By substituting equation 6 into equation 4, one can obtain the energy release rate associated with the crack progression in the 2D DCM model as shown in Fig. 17b. The figure shows a good agreement of the energy release rate approximation obtained using equation 6 and the Peach-Koehler (PK) force on the leading dislocation dipole that represent the crack tip. It is worth mentioning that PK force on the leading dislocation dipole is equivalent to the J-integral (please see reference Sheng et al. (2018) for details).

For additional verification and comparison, a 3D contact problem of the DC test was developed using the FEM computer program COMSOL. The boundary conditions were applied as shown in Fig. 19a. A semielliptical crack (a= 1.65 mm, c = 4 mm) was introduced in the geometry and meshed with 3724 quad elements. By adding a J-Integral sub-node, the crack tip boundary was selected, as shown in Fig. 19b. Comparing the elastic field obtained by both COMSOL and 3D DCM for the initial crack, one can conclude that the results are in good agreement, as shown in Fig. 20. The SIF and energy release rates (J-integral) around the crack

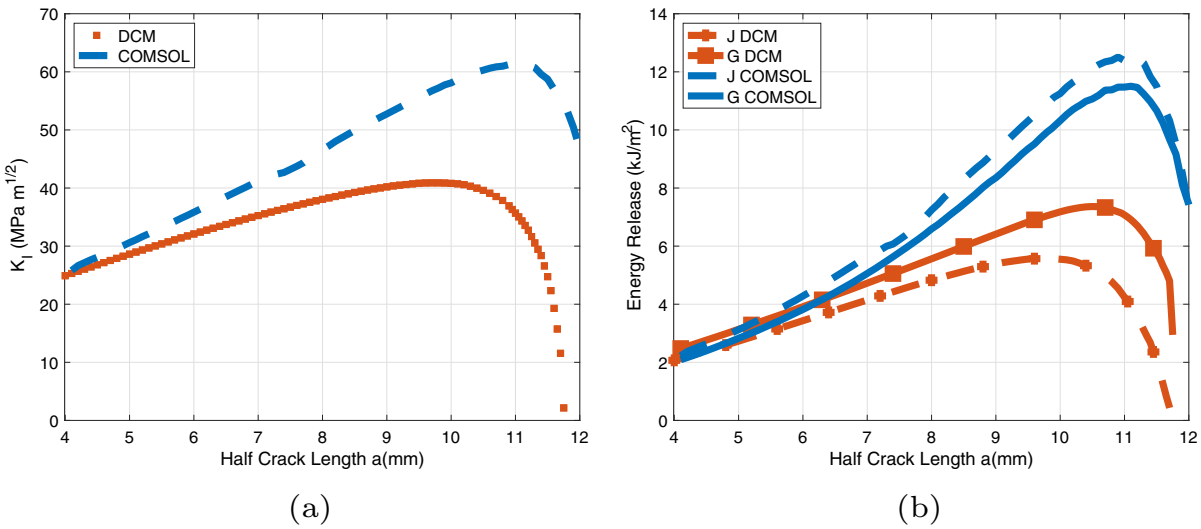

Fig. 17 **a** Stress intensity factor evolution calculated using 2D DCM model compared to COMSOL numerical solution. **b** Energy release rate evolution calculated using the 2D DCM model and compared to the COMSOL numerical solution

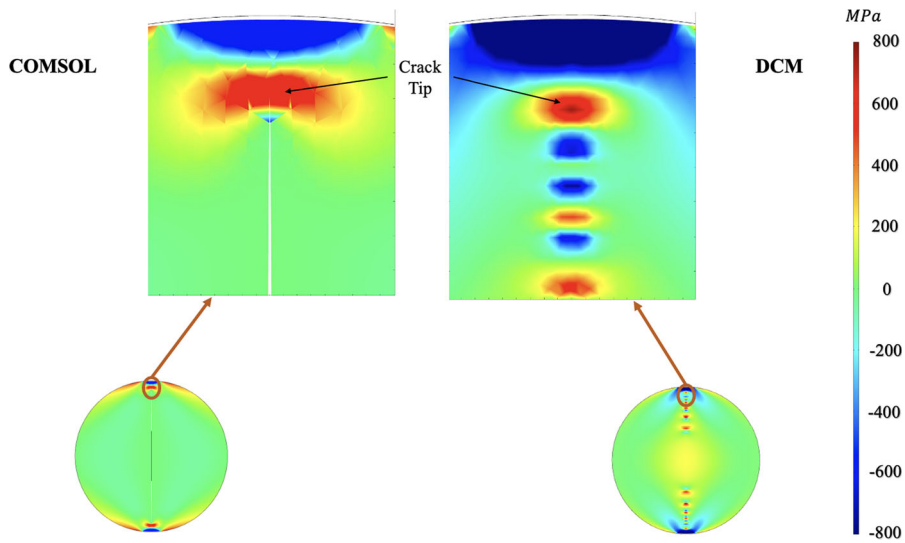

Fig. 18 Comparison of the stress field component σ_{xx} obtained by COMSOL and 2D DCM at the final stage of crack propagation (2a = 11.6 mm)

tip were numerically calculated, as shown in Fig. 21. Similar to the Carpinteri comparison (Fig. 14a), The SIF in Fig. 21a shows a discrepancy at the crack tips (x/c=0 & x/c=l) while at the middle region $0 < x/c \leq 1$ the calculated SIF is in good agreement.

To further ascertain the results, Carpinteri's analytical approximation of a semi-elliptical crack in a plate under tension was used as a reference and the SIF around the crack tip boundary was compared with a solution obtained from COMSOL and 3D DCM as shown in Fig. 14a. The results indicate that the SIF obtained with the 3D DCM model is in good agreement with Carpinteri analytical approximation at the regions $0 < x/c \leq 1$. On the other hand, the solution obtained from COMSOL shows good agreement at the crack tip x/c=0, however it diverges from Carpinteri's approximation with a relative error of approximately 37% in the region $0 < x/c \leq 1$ as shown in Fig. 14b. These calculations confirm that our developed DFM model is accurate for calculations of the SIF and hence the fracture toughness in the DC test. It is important to note that while good agreement is obtained with a purely

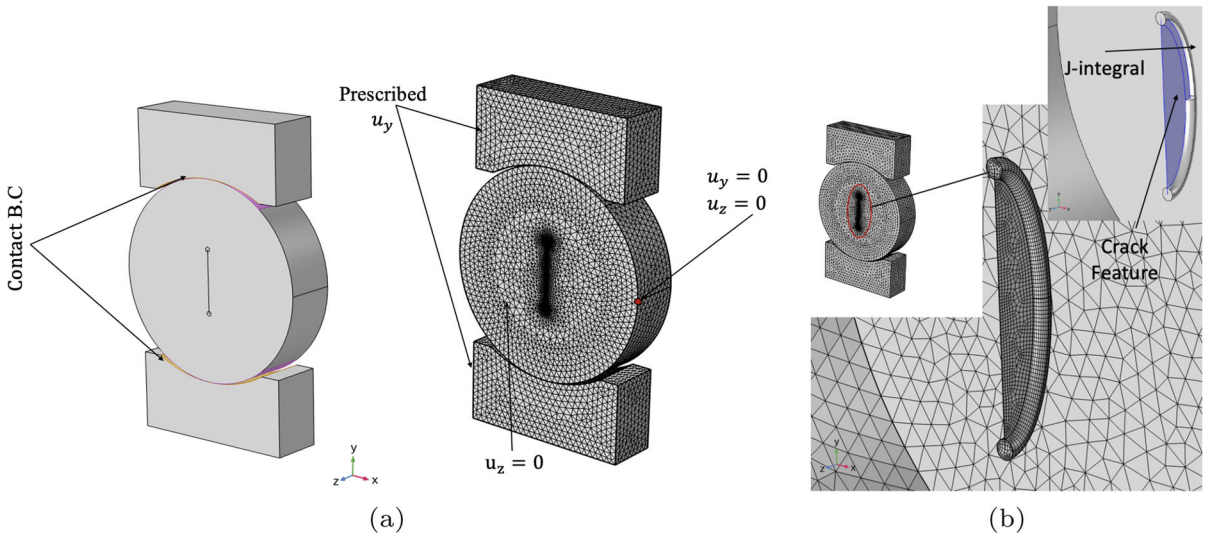

Fig. 19 **a** Boundary conditions applied to the 3D COMSOL model. **b** Meshed crack and the applied boundary conditions on the crack surface

FEM method, as we demonstrated using COMSOL, this agreement is possible as along as the crack tips are away from the disk boundaries. As the crack tips approach the disk boundaries before the crack stops, our DCM method is far superior in its accuracy, since the crucial stress singularity at the crack tips is inherently accurate in our DFM approach.

5 Conclusions

Accurate measurement of the fracture toughness is difficult for ceramics because of several reasons. First, tensile specimens are not generally usable because they are hard to prepare and they are prone to fracture at the grips. Second, bending tests introduce a spatially nonuniform stress field that can make interpretation of the fracture toughness data difficult. Third, a large variation of the fracture toughness is generally found, depending on the level of porosity and initial flaw size distribution. In the case of alumina, there are nine grades (A1–A9) with an increasing porosity content. Fracture toughness values are reported to be in the range $3--6\,\mathrm{MPa}\sqrt{\mathrm{m}}$ for A1 grades (0.2–3% porosity) down to $2.5--3.5\,\mathrm{MPa}\sqrt{\mathrm{m}}$ for A9 (3–6% porosity) Auerkari (1996). The samples we tested here had even greater porosity, up to 25%, and hence are expected to have lower fracture toughness values. The current measurement technique gave a value of $1.99\,\mathrm{MPa}\sqrt{\mathrm{m}}$ from 3D simulations, and $2.1\,\mathrm{MPa}\sqrt{\mathrm{m}}$ from 2D simulations.The effects of porosity were implicitly included through the measured value of the elastic modulus and the local resistance to slow crack growth. As the alumina porosity increase, the ceramic stiffness decreases Auerkari (1996), which implicitly reflects a decrease in the fracture toughness.

We demonstrated here that solutions based on a purely FEM analytical approaches to the disk compression problem are not adequate for measurement of low fracture toughness. The main reason is that these solutions become increasingly inaccurate as the crack tips approach the disk boundaries because of strong image forces on the crack tip and the need to adequately satisfy the imposed contact problem boundary conditions. Since SIF values for small initial size cracks at the disk center are high, the crack must propagate to approach disk boundaries and release the stored elastic energy in the disk. When the SIF is equal to the fracture toughness at the crack tip, the net PK force is zero and the crack stops. However, this often happens when the crack tip is near the disk boundary, thus demanding our high accuracy discrete fracture mechanics (DCM) model. The DCM has shown that it can accurately predict the fracture toughness form the relationship between the crack arrest position and the imposed loading displacement in a diametral compression test. Thanks to the mesh independence and crack representation with Volterra dislocations, DCM has been shown to outperform the

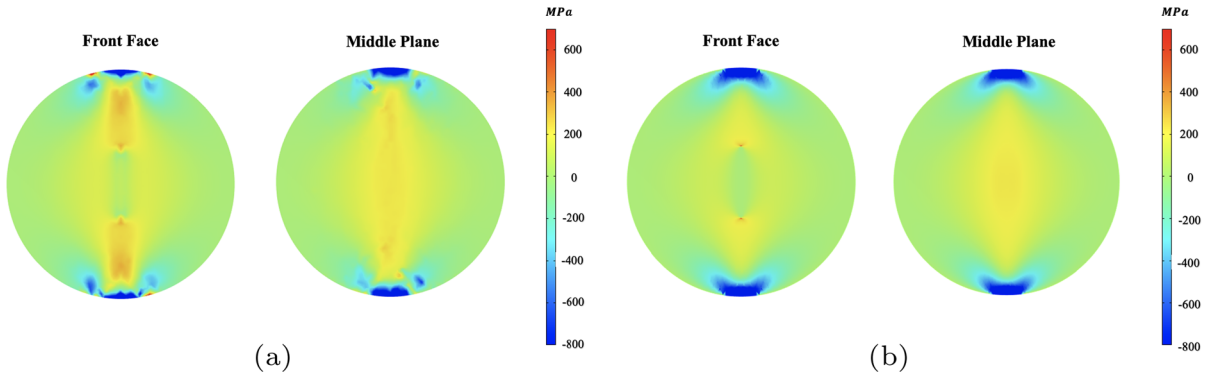

Fig. 20 Crack opening stress component σ_{xx} for the initial crack obtained from DCM (**a**) and COMSOL (**b**)

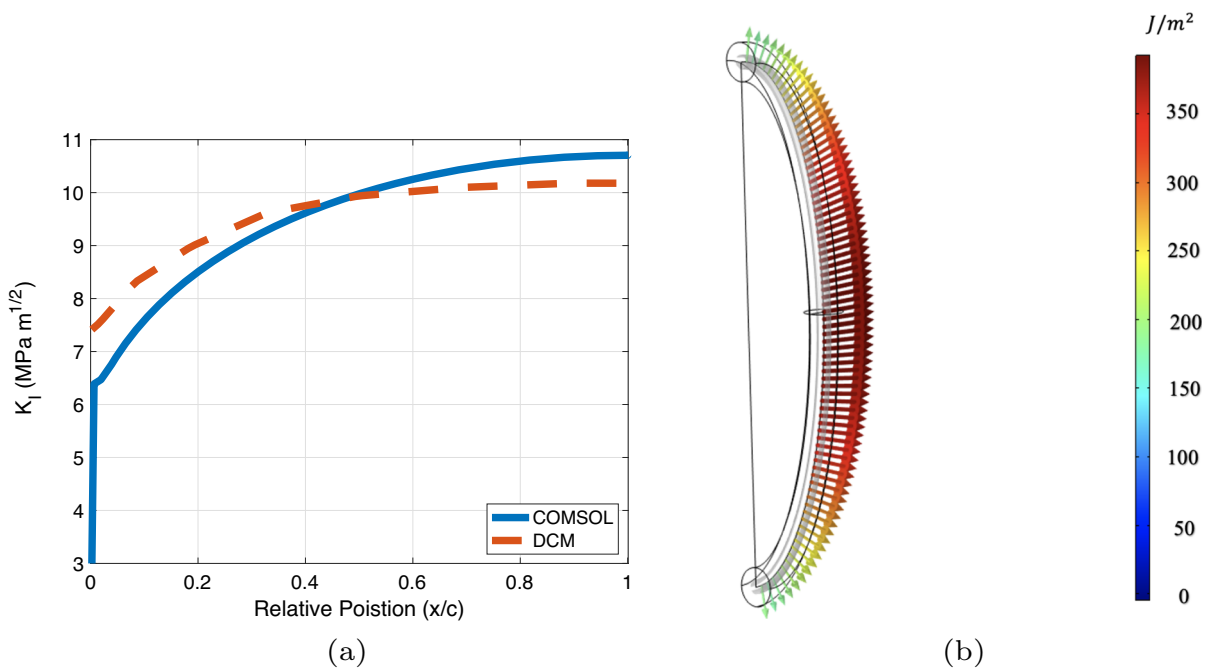

Fig. 21 Comparison of the stress intensity factor of the initial crack calculated along the crack using 3D DCM and COMSOL (**a**) J integral distribution along the crack surface obtained from COMSOL numerical solution at the initial configuration (**b**)

conventional FEM method in measuring the fracture toughness of ceramic materials. The precise near tip stress field of the Volterra dislocation array, coupled with the mesh-independence during crack propagation are important factors that enable measurement of very low fracture toughness of brittle materials.

Acknowledgements This work was supported by the U.S. Department of Energy, Office of Fusion Energy Sciences, under Award Number DE-SC0018410 with UCLA.

References

Auerkari P (1996) Mechanical and physical properties of engineering alumina ceramics, vol 23. Technical Research Centre of Finland Espoo

Awaji H, Sato S (1978) Combined mode fracture toughness measurement by the disk test. J Eng Mater Technol 100:175–182

Awaji H, Sato S (1979) Diametral compressive testing method. J Eng Mater Technol 101(2):139–147

Blaber J, Adair B, Antoniou A (2015) Ncorr: open-source 2d digital image correlation matlab software. Exp Mech 55(6):1105–1122

Carpinteri A (1991) Stress-intensity factors for semi-elliptical surface cracks under tension or bending. Eng Fract Mech 38(4–5):327–334

Clobes J, Green D (2002) Validation of single-edge v-notch diametral compression fracture toughness test for porous alumina. J Mater Sci 37(12):2427–2434

Croquelois B, Kopp J, Girardot J, Tchoreloff P, Mazel V (2021) Dynamic fracture analysis in Brazilian test: application to pharmaceutical tablets. Int J Fracture 229(1):113–124

Eshelby J (1982) Aspects of the theory of dislocations. Mechanics of solids. Elsevier, Amsterdam, pp 185–225

Eshelby J, Frank F, Nabarro F (1951) Xli. The equilibrium of linear arrays of dislocations. Lond Edinb Dublin Philos Mag J Sci 42(327):351–364

Es-Saheb MH, Albedah A, Benyahia F (2011) Diametral compression test: validation using finite element analysis. Int J Adv Manuf Technol 57(5):501–509

Fahad M (1996) Stresses and failure in the diametral compression test. J Mater Sci 31(14):3723–3729

Ghoniem NM, Huang J (2006) The elastic field of general-shape 3-d cracks. Philos Mag 86(27):4195–4212

Ghoniem NM, Tong S-H, Sun L (2000) Parametric dislocation dynamics: a thermodynamics-based approach to investigations of mesoscopic plastic deformation. Phys Rev B 61(2):913

Gopalakrishnan K, Mecholsky JJ (2012) Quantitative fractography of mixed-mode fracture in soda lime silica glass. J Am Ceram Soc 95(11):3622–3627

Jonsén P, Häggblad H-Å, Sommer K (2007) Tensile strength and fracture energy of pressed metal powder by diametral compression test. Powder Technol 176(2–3):148–155

Liu C, Woznick C, Scott S, Duque A, Herman M, Yeager J (2021) Brazilian disk compression testing of plastic-bonded idoxuridine mock explosive. J Energetic Mater 1–32

Mazel V, Guerard S, Croquelois B, Kopp J-B, Girardot J, Diarra H, Busignies V, Tchoreloff P (2016) Reevaluation of the diametral compression test for tablets using the flattened disc geometry. Int J Pharm 513(1–2):669–677

Newton C, Jeffs S, Gale L, Pattison S, Bache M (2022) Determining the interlaminar tensile strength of a sicf/sic ceramic matrix composite through diametrical compression testing. J Eur Ceram Soc

Sabri M, Ghazvinian A, Nejati HR (2016) Effect of particle size heterogeneity on fracture toughness and failure mechanism of rocks. Int J Rock Mech Min Sci 81:79–85

Sheity DK, Rosenfield AR, Duckworth WH (1985) Fracture toughness of ceramics measured by a chevron-notch diametral-compression test. J Am Ceram Soc 68(12):C–325

Sheng A, Ghoniem NM, Crosby T, Po G (2018) A mesh-independent method for three-dimensional crack growth in finite geometry. Int J Numer Methods Eng 117:38–62

Shin C, Cai C (2004) Experimental and finite element analyses on stress intensity factors of an elliptical surface crack in a circular shaft under tension and bending. Int J Fract 129(3):239–264

Solutions C (2020) Angle Crack Embedded in a Plate. https://www.comsol.com/model/download/835091/models.sme.angle_crack_plate.pdf

Solutions C, Speckle Pattern Fundamentals. Correlated Solutions. Correlated Solutions

Swab JJ, Yu J, Gamble R, Kilczewski S (2011) Analysis of the diametral compression method for determining the tensile strength of transparent magnesium aluminate spinel. Int J Fract 172(2):187–192

Szendi-Horvath G (1980) Fracture toughness determination of brittle materials using small to extremely small specimens. Eng Fracture Mech 13(4):955–961

Takahashi A, Ghoniem NM (2013) Fracture mechanics of propagating 3-d fatigue cracks with parametric dislocations. Philos Mag 93(20):2662–2679

Yan X (2006) Numerical analysis of the stress intensity factor for two kinds of mixed-mode crack specimens. J Strain Anal Eng Design 41(1):9–18

Zakavi B, Kotousov A, Branco R (2022) Overview of three-dimensional linear-elastic fracture mechanics. Int J Fract 234(1):5–20

Zaytsev D, Panfilov P (2014) Deformation behavior of human dentin in liquid nitrogen: a diametral compression test. Mater Sci Eng C 42:48–51